ETV4 promotes metastasis in response to activation of PI3-kinase and Ras signaling in a mouse model of advanced prostate cancer

Alvaro Aytes[a,b,c], Antonina Mitrofanova[b,d], Carolyn Waugh Kinkade[a,b], Celine Lefebvre[b,d], Ming Lei[b,e], Vanessa Phelan[a,b], H. Carl LeKaye[f], Jason A. Koutcher[f], Robert D. Cardiff[g], Andrea Califano[b,d], Michael M. Shen[b,d,e], and Cory Abate-Shen[a,b,d,1]

[a]Department of Urology and Department of Pathology and Cell Biology, [b]Herbert Irving Comprehensive Cancer Center, [d]Department of Systems Biology, and [e]Department of Medicine and Department of Genetics and Development, Columbia University Medical Center, New York, NY 10032; [c]Translational Research Laboratory, Catalan Institute of Oncology, Bellvitge Institute for Biomedical Research, L'Hospitalet de Llobregat, 08907 Barcelona, Spain; [f]Department of Medical Physics, Medicine, and Radiology, Memorial Sloan–Kettering Cancer Center, New York, NY 10065; and [g]Center for Comparative Medicine and Department of Pathology, School of Medicine, University of California, Davis, CA 95616

Edited by Frank J. Rauscher, The Wistar Institute, Philadelphia, PA, and accepted by the Editorial Board July 9, 2013 (received for review February 24, 2013)

Combinatorial activation of PI3-kinase and RAS signaling occurs frequently in advanced prostate cancer and is associated with adverse patient outcome. We now report that the oncogenic *Ets* variant 4 (*Etv4*) promotes prostate cancer metastasis in response to coactivation of PI3-kinase and Ras signaling pathways in a genetically engineered mouse model of highly penetrant, metastatic prostate cancer. Using an inducible Cre driver to simultaneously inactivate *Pten* while activating oncogenic *Kras* and a fluorescent reporter allele in the prostate epithelium, we performed lineage tracing in vivo to define the temporal and spatial occurrence of prostate tumors, disseminated tumor cells, and metastases. These analyses revealed that though disseminated tumors cells arise early following the initial occurrence of prostate tumors, there is a significant temporal lag in metastasis, which is temporally coincident with the up-regulation of *Etv4* expression in primary tumors. Functional studies showed that knockdown of *Etv4* in a metastatic cell line derived from the mouse model abrogates the metastatic phenotype but does not affect tumor growth. Notably, expression and activation of *ETV4*, but not other oncogenic *ETS* genes, is correlated with activation of both PI3-kinase and Ras signaling in human prostate tumors and metastases. Our findings indicate that *ETV4* promotes metastasis in prostate tumors that have activation of PI3-kinase and Ras signaling, and therefore, *ETV4* represents a potential target of therapeutic intervention for metastatic prostate cancer.

Metastasis is a highly inefficient process that involves multiple steps, including invasion of local stroma, intravasation into the bloodstream and/or lymphatic system, and extravasation into a secondary tissue, which is thought to arise as a consequence of multiple molecular/epigenetic alterations in tumor cells, as well as in the microenvironment of metastatic sites (1–4). Nonetheless, despite its inefficiency, most cancer deaths are due to metastases and our current inability to treat them once they arise. In particular, in prostate cancer, the locally invasive disease has a nearly 100% survival rate, whereas metastatic prostate cancer is very often lethal (5).

Recent analyses have identified key molecular pathways that are frequently dysregulated during prostate cancer progression, as a consequence of copy number alterations, chromosomal rearrangements, and other aberrant genetic/epigenetic events (6–10). For example, loss of chromosomal region 8p21 and coincident haploinsufficiency for the *NKX3.1* homeobox gene occurs frequently in precursor lesions known as prostatic intraepithelial neoplasia (PIN) and are associated with prostate cancer initiation (11, 12). Another early event in prostate tumorigenesis is the formation of the *TMPRSS2–ERG* rearrangement, which fuses the transmembrane protease *TMPRSS2* promoter with the coding region of the *ETS* transcription factor *ERG* (13, 14). The *TMPRSS2–ERG* fusion is highly prevalent in prostate cancer and is associated with disease outcome in some cases (13, 15), and functionally cooperates with dysregulation of other key genes, including the *PTEN* tumor suppressor, in prostate cancer progression (16-19). Notably, other oncogenic *ETS* genes (20), including *ETV1*, undergo translocation in prostate cancer and collaborate with *PTEN* in cancer progression (21-23), and at least one tumor-suppressive *ETS* family member, *ETS2*, is mutated in advanced prostate cancer (8). Despite these findings, the complexity of *ETS* gene function during prostate cancer progression has not been fully resolved.

At all disease stages, prostate cancer progression is critically dependent on androgen receptor signaling. As a consequence, depletion of testicular androgens initially leads to tumor regression, but this ultimately results in a castration-resistant disease that is highly metastatic and often fatal (24). Among key signaling pathways frequently dysregulated in advanced prostate cancer, the PI3-kinase and the Ras signaling pathways are each altered in ~40% of primary tumors, but nearly 90% of metastatic tumors (6). Consistent with their relevance for advanced disease, both the PI3-kinase and the Ras signaling pathways are func-

Significance

Although locally invasive prostate cancer is nearly always curable, metastatic prostate cancer usually results in lethality. Our study investigates the temporal progression and molecular mechanisms underlying prostate cancer metastasis using a new genetically engineered mouse model. Using lineage-tracing analyses, we show that dissemination of tumor cells occurs early in cancer progression, and well before the occurrence of metastases. We further show that metastasis is temporally coincident with expression of the oncogenic *ETS* gene *Etv4*, and that *Etv4* promotes prostate cancer metastasis in vivo. Our findings suggest that *Etv4* may be a target for therapeutic intervention in metastatic prostate cancer.

Author contributions: A.A., A.M., C.W.K., and C.A.-S. designed research; A.A., A.M., C.W.K., C.L., M.L., V.P., H.C.L., J.A.K., and R.D.C. performed research; A.A., A.M., A.C., and M.M.S. contributed new reagents/analytic tools; A.A., A.M., C.W.K., C.L., J.A.K., A.C., M.M.S., and C.A.-S. analyzed data; and A.A., A.M., M.M.S., and C.A.-S. wrote the paper.

The authors declare no conflict of interest.

This article is a PNAS Direct Submission. F.J.R. is a guest editor invited by the Editorial Board.

Data deposition: The microarray data reported in this paper have been deposited in the Gene Expression Omnibus (GEO) database, www.ncbi.nlm.nih.gov/geo (accession no. GSE47697).

See Commentary on page 14819.

[1]To whom correspondence should be addressed. E-mail: cabateshen@columbia.edu.

This article contains supporting information online at www.pnas.org/lookup/suppl/doi:10.1073/pnas.1303558110/-/DCSupplemental.

Downloaded at Palestinian Territory, occupied on November 26, 2021

www.manaraa.com

tionally associated with castration-resistant prostate cancer (25–27). Ample evidence has shown that loss of function of *PTEN* is principally responsible for activation of the PI3-kinase pathway in prostate cancer (12, 28). In contrast, the mechanisms leading to activation of Ras signaling have been more difficult to resolve (29), in part because mutations of the *KRAS* oncogene are infrequent in prostate cancer (30–33), and because chromosomal rearrangements involving *KRAS* activation in advanced prostate cancer are also rare (10, 34).

In the current study, we show that the *Ets* gene *Etv4* is activated in response to PI3-kinase and Ras signaling in a mouse model of metastatic prostate cancer. Using lineage tracing in a genetically engineered mouse model in vivo, we elucidate the temporal relationship between the initial appearance of prostate cancer phenotypes and the occurrence of metastases. We show that *Etv4* is expressed in primary tumors and metastases, and demonstrate that *Etv4* is required for metastasis using cell culture and in vivo assays. Our findings demonstrate that combinatorial activation of PI3-kinase and Ras signaling promotes prostate cancer metastasis through activation of *Etv4*.

Results

Combined Activation of PI3-Kinase and Ras Signaling Pathways Is Associated with Metastatic Prostate Cancer in Humans and a Genetically Engineered Mouse Model. Given the observation that the PI3-kinase and Ras signaling pathways are often activated in a significant percentage of advanced primary prostate tumors and metastases (6), we asked whether they were coordinately activated in such tumors. We found that dysregulation of PI3-kinase and Ras signaling pathways are significantly correlated ($P = 1.2 \times 10^{-7}$) in human prostate tumors and particularly in metastases (Fig. 1*A*). Furthermore, coactivation of PI3-kinase and Ras signaling pathways is significantly associated with adverse patient outcome in two independent human prostate cancer cohorts using biochemical recurrence (BCR)-free survival ($P = 0.003$) (6) and prostate cancer-specific survival ($P = 0.014$) (35) as disease endpoints (Fig. 1*B*).

To combinatorially activate these signaling pathways in genetically engineered mice (Fig. 2), we used a *Nkx3.1*^{CreERT2} knock-in allele (36), which simultaneously inactivates the *Nkx3.1* homeobox gene while driving tamoxifen-inducible Cre-mediated recombination in luminal prostate epithelium, thus enabling spatial and temporal control of Cre activity. To activate PI3-kinase signaling, we used a *Pten* floxed allele (37), and because the mechanisms leading to activation of Ras signaling in human prostate cancer are still unresolved (Introduction), we used a well-characterized conditional oncogenic *Kras* (*Kras*$^{LSL\text{-}G12D/+}$) allele (38).

Following tamoxifen induction, the resulting *Nkx3.1*$^{CreERT2/+}$;*Pten*$^{flox/flox}$;*Kras*$^{LSL\text{-}G12D/+}$ mice (hereafter denoted *NPK* mice) develop lethal prostate cancer (i.e., 50% survival at 101 d; $P < 0.0001$), in striking contrast to mice having inactivation of *Pten* but lacking activation of *Kras* (*Nkx3.1*$^{CreERT2/+}$;*Pten*$^{flox/flox}$; hereafter denoted *NP* mice), which rarely succumb to the disease (Fig. 2*S*; *SI Appendix*, Table S1). The *NPK* mice developed large prostate tumors with prominent invasive adenocarcinoma, whereas the *NP* mice primarily display high-grade PIN and in situ carcinoma that progresses to adenocarcinoma in aged mice (Fig. 2 *A–L*, *T*, and *V*; *SI Appendix*, Fig. S1 and Table S1). Interestingly, mice having activated *Kras* but not *Pten* inactivation (i.e., *Nkx3.1*$^{CE2/+}$;*Kras*$^{LSL\text{-}G12D/+}$; hereafter, *NK* mice) displayed histopathology within normal limits (*SI Appendix*, Fig. S1 *H* and *L* and Table S1), indicating that the consequences of *Kras* activation in the prostate are latent when *Pten* is wild type. Notably, the *NPK* tumors are highly proliferative, express nuclear androgen receptor (AR), and are primarily comprised of luminal epithelial cells (Fig. 2 *M–R*, *U*, and *W*). These findings are similar to those of a previous study using a constitutive Cre allele for inactivation of *Pten* while activating *Kras* in the prostate (39).

To identify the genes/molecular pathways that may contribute to the aggressive phenotype of the *NPK* mice, we performed gene expression profiling to compare the *NPK* and *NP* prostate tumors ($n = 8$ per group; *SI Appendix*, Fig. S2*A* and Dataset S1). Among genes significantly up-regulated in the *NPK* tumors were *c-Fos* ($P < 0.0001$), which is activated in response to Ras signaling and associated with poor outcome in prostate cancer (40), and *Ezh2* ($P < 0.0001$), which has been shown to activate Ras signaling in prostate cancer metastases by silencing a Ras GTPase-activating protein (41) (*SI Appendix*, Fig. S2*B*). Interestingly, among genes significantly down-regulated in the *NPK* tumors were two putative metastasis suppressors, *Rkip* ($P < 0.001$) and *Nm23* ($P < 0.0001$; *SI Appendix*, Fig. S2*B*). Furthermore, analyses of biological pathways using gene-set enrichment analysis (GSEA) (42) revealed that pathways significantly ($P < 0.008$) up-regulated in the *NPK* vs. *NP* mouse prostate tumors include cell cycle, mitosis, p53 pathway, steroid biosynthesis, focal adhesion, and extracellular receptor interaction (Fig. 3*A*; *SI Appendix*, Fig. S2*C* and Dataset S2). Consistent with the latter

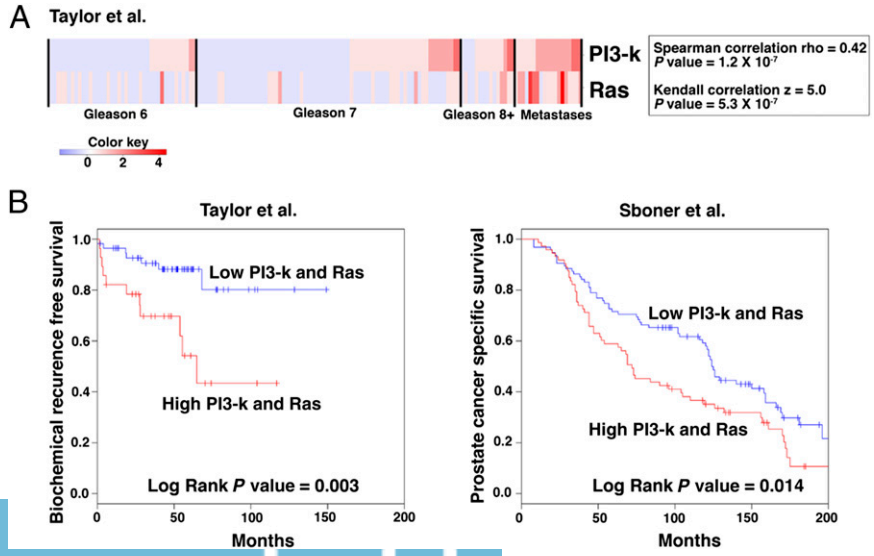

Fig. 1. Coactivation of PI3-kinase and Ras signaling pathways is associated with adverse patient outcome. (*A*) Correlation of PI3-kinase and Ras signaling in human prostate cancer from the Taylor et al. (6) dataset. Shown is a heat map in which each clinical sample (i.e., primary tumors of the indicated Gleason scores and metastases) was evaluated to determine status for PI3-kinase and Ras signaling (*Materials and Methods*). Correlation coefficients and *P* values of the correlations are shown for both Spearman rho and Kendall z calculations. The color key indicates relative expression levels of the pathway. (*B*) Kaplan–Meier analyses showing the association of activation of both PI3-kinase and Ras signaling with adverse patient outcome in two independent cohorts using biochemical recurrence-free (BCR-free; *Left*) and prostate cancer-specific survival (*Right*) as clinical endpoints.

PNAS PLUS
SEE COMMENTARY
MEDICAL SCIENCES
Downloaded at Palestinian Territory, occupied on November 26, 2021
www.manaraa.com

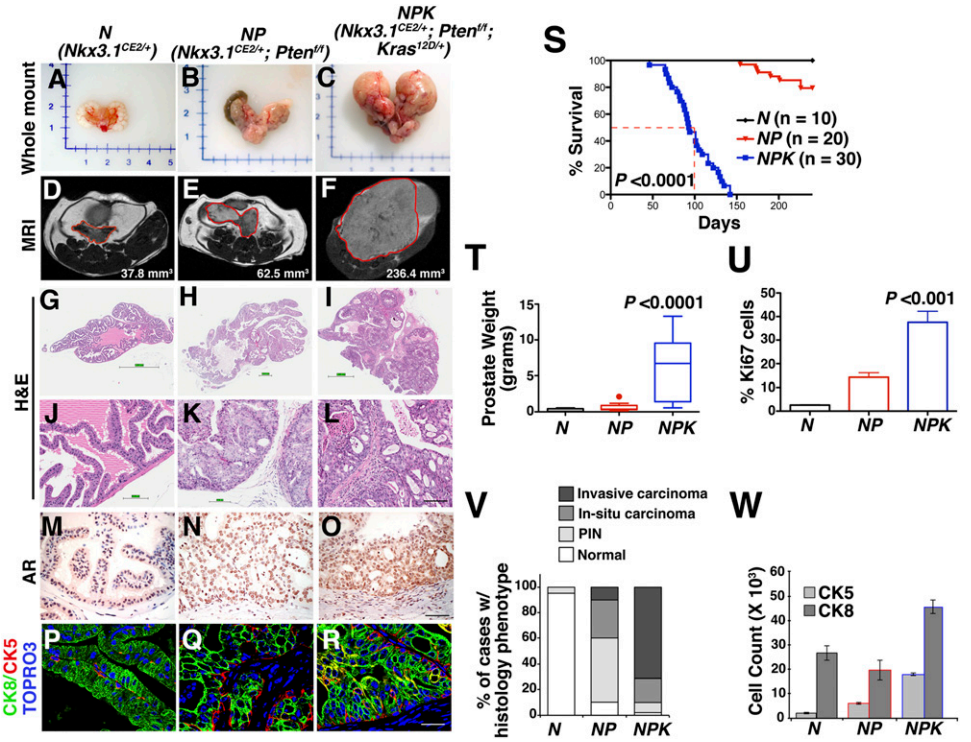

Fig. 2. Cooperation of PI3-kinase and Ras signaling pathways in advanced prostate cancer in a genetically engineered mouse model. Mice of the indicated genotypes were induced with tamoxifen at 2 mo and analyzed at 8 (for *N*), 9 (for *NP*), or 4 (for *NPK*) mo after induction. (*A–C*) Whole-mount images. (*D–F*) MRI images with the regions corresponding to prostate indicated by the red lines and with tumor volumes indicated. (*G–L*) Representative H&E images of anterior prostate showing whole-slide (*G–I*) or high-power (*J–L*) images. (*M–O*) Immunohistochemical staining for AR. (*P–R*) Immunofluorescence images show staining for cytokeratin 8 (CK8), which stains luminal epithelium, and cytokeratin 5 (CK5), which stains basal cells. (*S*) Survival curve showing the percent of mice of the indicated genotypes remaining alive relative to days after tumor induction with tamoxifen; for the *NPK* mice, 50% survival is indicated by the dashed red line. (*T*) Average wet weights of anterior prostate (*N*) or prostate tumors (*NP* and *NPK*). (*U*) Average proliferation assessed by the number of Ki67-positive cells relative to the total number of epithelial cells. (*V*) Summary of the histopathological phenotype. (*W*) Quantification of CK8 and CK5 immunofluorescence staining. *P* values compare *NPK* mice to the control (N, normal prostate). (Scale bars, 100 μm.) Additional supporting data are provided in *SI Appendix*, Fig. S1 and Table S1.

being associated with epithelial–mesenchymal transition (EMT), direct evidence of EMT in the *NPK* tumors was apparent by immunofluorescence staining and real-time PCR for relevant markers, including reduced expression of E-cadherin, and elevated expression of Snail and fibronectin (*SI Appendix*, Fig. S3 *A–D*). Thus, *NPK* tumors display molecular features associated with advanced prostate cancer.

To directly compare the molecular profile of *NPK* mouse tumors with that of advanced human prostate cancer, we performed GSEA using a reference gene signature from human prostate cancer representing malignant tumors with Gleason 8 and higher and less than 3 y to biochemical recurrence, (n = 10) vs. indolent tumors having Gleason 6 and that did not recur (n = 39) (6). Cross-species GSEA of genes differentially expressed in the *NPK* vs. *NP* mouse prostate tumors with the reference signature of malignant vs. indolent human prostate cancer revealed that genes up-regulated in the *NPK* mouse tumors were more frequently expressed in the malignant human tumors [normalized enrichment score (NES) = 3.36; P = 0.012], and conversely genes that were down-regulated in the *NPK* mouse tumors were more frequently expressed in the indolent human tumors (NES = −4.15; P < 0.001; Fig. 3*B*; *SI Appendix* and Dataset S3). Furthermore, GSEA of biological pathways enriched in the human malignancy signature also revealed a significant enrichment in the pathways activated in *NPK* vs. *NP* mouse signature (NES = 4.49, P = 0.001; Fig. 3*C*). Together these findings demonstrate a striking conservation of both gene expression and biological pathways in *NPK* mouse prostate tumors with advanced human prostate cancer.

Furthermore, the *NPK* vs. *NP* tumor signature was significantly enriched for both activated PI3-kinase and Erk/MAP kinase signaling pathways (P = 0.004 and P < 0.001, respectively; Fig. 3*A*; *SI Appendix*, Fig. S2*C* and Dataset S2), which was further apparent by immunohistochemical and Western blot analyses (Fig. 3 *D–P*). Of particular note was the robust (~10-fold) increase in phosphorylation of the winged-helix transcription factor FoxO3a (p-FoxO3a) at threonine 32 (Fig. 3 *D–P*), presumably a consequence of Ras-mediated activation of Akt kinase (43); phosphorylation of FoxO3a is known to abrogate its tumor suppressive activity (44). Thus, the *NPK* prostate tumors have activation of relevant signaling pathways.

Consistent with their molecular characteristics, as well as their poor survival (Fig. 2*S*), all of the *NPK* mice (n = 15/15), but none of the *NP* mice (n = 0/16), displayed visible metastases, primarily to lungs and liver, but also to diaphragm, pancreas, kidney, and proximal lymph nodes (Fig. 4 *A–G*; *SI Appendix*, Fig. S4 *A–E* and Table S1). Notably, the essentially 100% penetrance of metastases in the *NPK* mice differ from the lower frequency of metastases in most other mouse models or prostate cancer (45), including an analogous model based on activated *B-Raf* oncogene in cooperation with loss of function of *Pten* (46). The visible metastases in the *NPK* mice were corroborated by histological analysis, and their prostate origin was verified with markers from the primary tumor (Fig. 4 *A–F* and *H–S*; *SI Appendix*, Fig. S4 *A–K* and Table S1). Notably, the high incidence of metastases was highly correlated with the detection of disseminated tumor cells (DTCs) isolated from the bone marrow of the *NPK* mice (n = 18/20), compared with the *NP* mice (n = 1/18; Fig. 4*G*; *SI Appendix*, Table S1), although we did not observe metastases to bone, which is a major site of metastasis in human prostate cancer (47). The metastases in both the lung and lymph nodes of the *NPK* mice were highly proliferative and displayed robust expression of various markers found in the primary tumor, including pan-cytokeratin and androgen receptor, as well as robust activation of PI3-kinase and MAP kinase pathways, including robust expression of p-FoxO3a (n = 5 per group; Fig. 4 *H–S*; *SI Appendix*, Fig. S4 *F–K*). In summary, *NPK* mice develop lethal, highly penetrant metastatic prostate cancer, which recapitulates key molecular features associated with advanced prostate cancer in humans.

Lineage-Tracing Analysis of the Spatial and Temporal Occurrence of Metastases. Given the highly penetrant metastatic phenotype of the *NPK* mice, we used the inducible *Nkx3.1*^{CreERT2} driver to lineage-

Downloaded at Palestinian Territory, occupied on November 26, 2021
www.manaraa.com

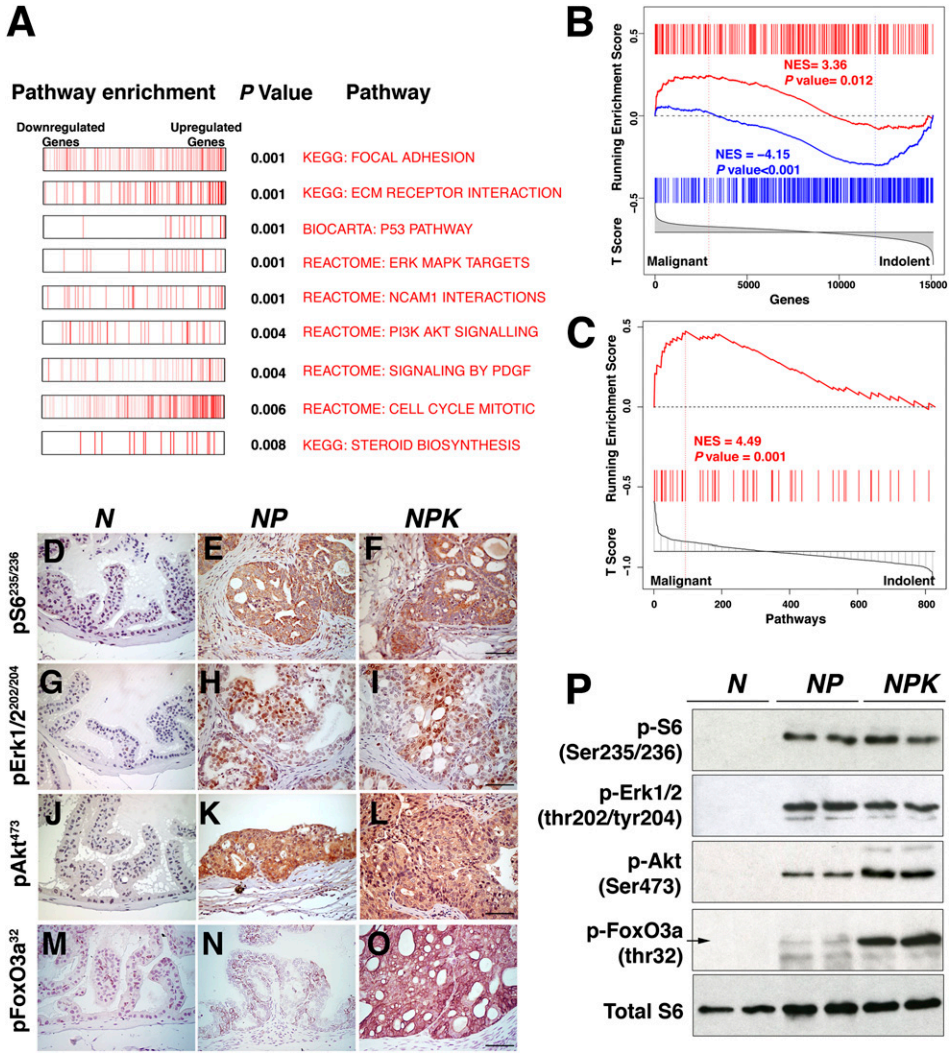

Fig. 3. Signaling pathway activation in *NPK* mouse prostate tumors. (*A*) Pathway enrichment analyses. Summary of GSEA analyses comparing *NPK* and *NP* mouse prostate tumors. Shown is a summary of biological pathways indicating the down-regulated and up-regulated genes, with *P* value of enrichment indicated. (*B*) Cross-species GSEA analyses showing the enrichment of an expression signature from the *NPK* vs. *NP* mouse prostate tumors compared with a reference signature of malignant vs. indolent human prostate cancer. (*C*) GSEA analyses of biological pathways comparing pathways that are differentially activated in the *NPK* vs. *NP* mouse prostate tumors with pathways enriched in a reference signature of malignant vs. indolent human prostate cancer. (*D–O*) Immunohistochemical staining of mouse prostate tissues using the indicated phosphoantibodies. (Scale bars, 100 μm.) (*P*) Western blot analyses using total protein extracts prepared from dorsal prostate or prostate tumors from the indicated mouse genotypes. Additional supporting data are provided in *SI Appendix*, Figs. S2 and S3 and Datasets S1–S3.

mark prostate epithelial cells to follow their dissemination and metastasis in vivo (Fig. 5*A*). In particular, we crossed the *NPK* mice with a Cre reporter *R26R-YFP*, which expresses YFP following Cre-mediated recombination (48), to generate *NPK-YFP* mice (*Nkx3.1*$^{CreERT2/+}$;*Pten*$^{flox/flox}$; *Kras*$^{LSL\text{-}G12D/+}$;*Rosa26*$^{LSL\text{-}YFP/+}$). As controls, we analyzed *NPK-YFP* mice that were not induced with tamoxifen (i.e., *NPK-YFP* mice administered corn oil) and therefore do not form tumors (*SI Appendix*, Fig. S1 *G* and *K*), as well as *NP-YFP* mice that were induced with tamoxifen, but form tumors that do not metastasize (Fig. 4 *A–G*). Notably, the *Nkx3.1*^{CreERT2} allele is highly specific for prostate epithelial cells and does not display any leaky expression in the absence of tamoxifen (Fig. 6 *B*, *H*, and *N*) (36). Therefore, Cre-mediated recombination of the *YFP* reporter indelibly marks prostatic epithelial cells, such that their dissemination to distant sites can be identified unambiguously by their lineage mark, and conversely, the presence of marked cells at distant sites indicates their prostate origin (Fig. 5*A*). Accordingly, following tamoxifen induction, both the *NPK-YFP* and *NP-YFP* mice displayed prominent ex vivo YFP fluorescence in the prostate (n = 7 mice; Fig. 5 *B*, *C*, *H*, and *I*); however, only the *NPK-YFP* mice displayed ex vivo fluorescence in nonprostatic tissues, including the lungs and liver, which overlay with morphologically visible metastases (n = 7 mice; Fig. 5 *D–G* and *J–M*).

We next examined the temporal relationship between the occurrence of prostate tumor phenotypes and metastasis in the *NPK-YFP* mice following tamoxifen induction (Fig. 6*A*). The *NPK-YFP* mice rapidly developed histological features associated with prostate cancer, including high-grade PIN with areas of invasion by as early as 2 wk (0.5 mo) after tamoxifen induction and adenocarcinoma by 1 mo (Fig. 6 *D–G*; *SI Appendix*, Fig. S4 *L–O*). In contrast, metastases in lungs were not observed until at least 3 mo after tamoxifen induction, as evident by gross morphology (Figs. 4*C* and 5*J*), as well as by the robust detection of YFP-marked cells in immunostained sections (n = 2,187/6,800 cells; five mice; Fig. 6 *J–M*; *SI Appendix*, Table S2). Notably, the temporal occurrence of metastasis was coincident with elevated expression of the EMT markers, Snail and fibronectin, in primary tumors 3 mo after tamoxifen induction compared with those at 1 mo after tamoxifen induction (*SI Appendix*, Fig. S3*E*).

Although we did not observe visible metastases in lungs of *NPK-YFP* mice before 3 mo following tamoxifen induction, we observed small clusters of YFP-positive cells by 2 mo (n = 401/7,095 cells; five mice; Fig. 6 *J–M* and *T*; *SI Appendix*, Table S2), which we infer are micrometastases (see below). We also observed rare, solitary YFP-positive cells by 1 mo following tamoxifen induction (n = 65/6265 cells; five mice; Fig. 6 *J–M* and *T*; *SI Appendix*, Table S2). Notably, such YFP-positive cells were never observed in lungs from the aged-matched noninduced *NPK-YFP* control (i.e., corn-oiled treated) mice (n = 0/2,891 cells; four mice) or in the *NP-YFP* mice (n = 0/2,158 cells; five

PNAS PLUS
SEE COMMENTARY
MEDICAL SCIENCES
Downloaded at Palestinian Territory, occupied on November 26, 2021
www.manaraa.com

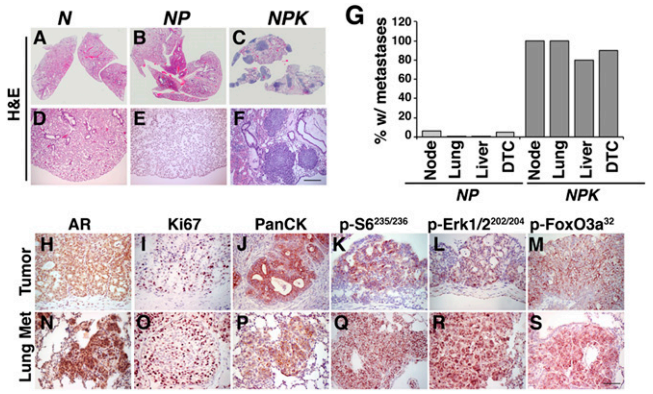

Fig. 4. Analyses of metastasis in *NPK* mice. (*A–F*) Representative H&E images of the lungs from the indicated mouse genotypes showing whole-slide (*A–C*) or high-power (*D–F*) images. (*G*) Summary of the incidence of metastases and DTCs in mice of the indicated genotypes. Metastases were scored by H&E analyses and immunostaining for AR and pan-cytokeratin; DTCs were quantified from bone marrow using real-time PCR (*Materials and Methods*). (*H–S*) Immunostaining for the indicated proteins/phosphoproteins comparing primary prostate tumors and lung metastases from the same *NPK* mice. Data show representative images from multiple ($n = 5$) comparisons of tumors and metastases from the corresponding mice. (Scale bars, 100 μm.) Additional supporting data are provided in *SI Appendix*, Figs. S3 and S4 and Table S1.

mice; Fig. 6 *H* and *I*; *SI Appendix*, Table S2). Furthermore, as early as 0.5 mo following tamoxifen induction, we detected YFP-expressing DTCs in bone marrow using a highly sensitive quantitative PCR assay (*SI Appendix*, Table S2). Additionally, YFP-positive cells were detectable in the proximal lymph nodes as early as 0.5 mo following tamoxifen induction (*SI Appendix*, Fig. S4 *P–S*). Together, these findings suggest that dissemination of prostate tumor cells in *NPK* mice occurs much earlier than the appearance of metastases.

Interestingly, although metastases from lungs and lymph nodes displayed robust expression of markers prevalent in the primary tumors, the solitary disseminated cells and the presumptive micrometastases had significantly lower levels of these markers. In particular, most of the YFP-expressing cells in the lung metastases in the 3-mo group were costained with cytokeratin 8 (94%; $n = 2{,}069/2{,}187$, five mice) and were highly proliferative (22%; $n = 619/2{,}750$, five mice; Fig. 6 *M*, *S*, *U*, and *V*; *SI Appendix*, Table S2), indicating their similarity to the prostate tumors from which they originate. In contrast, only 24% of the solitary YFP-expressing cells in the 1-mo group coexpress cytokeratin 8 ($n = 16/65$, five mice), whereas in the 2-mo group, 80% of YFP-expressing cells coexpressed cytokeratin 8 ($n = 321/401$, five mice; Fig. 6 *K*, *L*, *U*, and *V*; *SI Appendix*, Table S2). Furthermore, whereas 5.2% of the YFP-expressing cells at 2 mo coexpressed Ki67 ($n = 21/401$, five mice), none of the solitary YFP-expressing cells at 1 mo were proliferative ($n = 0/21$, five mice; Fig. 6 *Q*, *R*, *U*, and *V*; *SI Appendix*, Table S2), suggesting that these solitary disseminated cells in the lung were mostly dormant. Thus, these lineage-tracing analyses have revealed that there is a temporal lag in the appearance of metastases, although dissemination of tumor cells is temporally coincident with the manifestation of primary tumor phenotypes. Furthermore, the solitary disseminated tumor cells that arise early in tumorigenesis are likely to be dormant.

Activation of *Etv4* by PI3-Kinase and Ras Signaling in Metastatic Prostate Cancer. The further implication of these findings is that *NPK* primary tumors are not immediately capable of metastasizing (i.e., at 1 mo following tamoxifen induction), but later (i.e., by 3 mo following tamoxifen induction) acquire the capability to metastasize. Thus, we reasoned that gene expression profiling comparing *NPK* prostate tumors at 3 mo vs. 1 mo (*SI Appendix* and Dataset S4) should identify genes specifically associated with metastasis. Indeed, these analyses revealed differential transcriptional activity of the *PEA3* subfamily of ETS transcription factors, which consist of *Etv1*, *Etv4*, and *Etv5*, in the 3-mo vs. 1-mo *NPK* tumors (Fig. 7 *A* and *B*; *SI Appendix* and Datasets S4 and S5). Notably, these ETS transcription factors have been previously implicated in mediating Ras signaling in prostate (49, 50) and other cancers (51, 52), as well as in regulation of EMT markers, including Snail (53, 54).

In particular, we found that Etv target genes, including *Ezh2* and *c-Fos*, were differentially expressed ($P = 0.001$) in the 3-mo vs. 1-mo *NPK* tumors (*SI Appendix* and Dataset S5). Furthermore, GSEA analysis showed that a gene signature consisting of human *ETV* transcriptional target genes was significantly enriched in the *NPK* vs. *NP* prostate tumors (NES = 5.47; $P < 0.001$), as well as in the 3-mo vs. 1-mo *NPK* tumors (NES = 2.98; $P = 0.0014$; Fig. 7 *A* and *B*). In contrast to the enrichment of *ETV* targets, *ERG* transcriptional target genes were not enriched when comparing either the *NPK* vs. *NP* tumors (NES = 2.0; $P = 0.12$), or the 3-mo vs. 1-mo *NPK* tumors (NES = –0.65; $P = 0.61$; *SI*

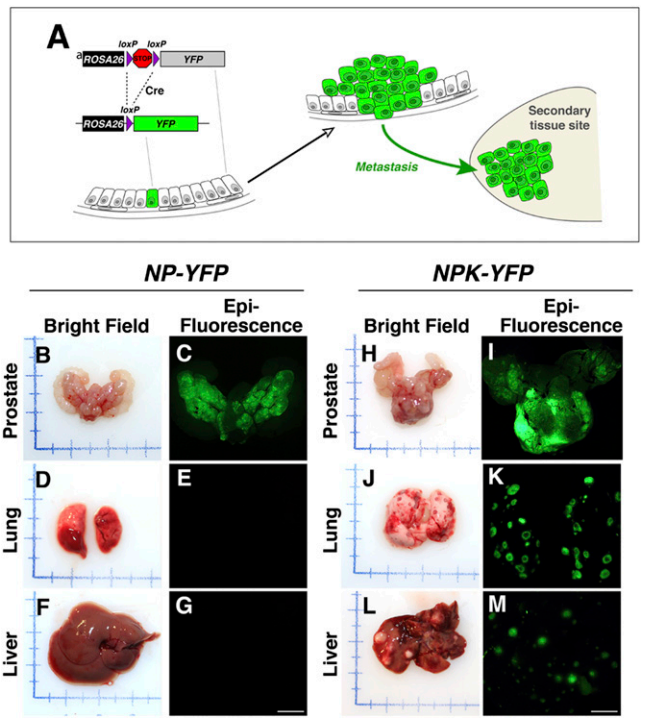

Fig. 5. Lineage-tracing analysis of metastases in vivo. (*A*) Strategy for lineage tracing of metastases with YFP. The *R26R* allele contains a *YFP* reporter under the control of the ubiquitously expressed *ROSA26* promoter, but is not expressed due to the presence of the transcriptional STOP sequence. Expression of Cre recombinase (shown here in a single cell) results in excision of the STOP sequence and expression of YFP. Cells descended from the original cell undergoing Cre-mediated recombination will be genetically marked by expression of YFP. If these cells metastasize to a distant site, they can be identified unambiguously by their lineage mark. (*B–M*) Corresponding bright-field and epifluorescence images showing prostate, lungs, and liver from mice of the indicated genotypes having a YFP (fluorescent) allele that is conditionally expressed in prostate following tamoxifen induction. Note that both *NP-YFP* and the *NPK-YFP* mice have robust fluorescence in the prostate, whereas only the *NPK-YFP* mice display metastatic lesions evident in the bright-field images of lungs and liver that display robust fluorescence. Additional supporting data are provided in *SI Appendix*, Fig. S4.

Downloaded at Palestinian Territory, occupied on November 26, 2021
www.manaraa.com

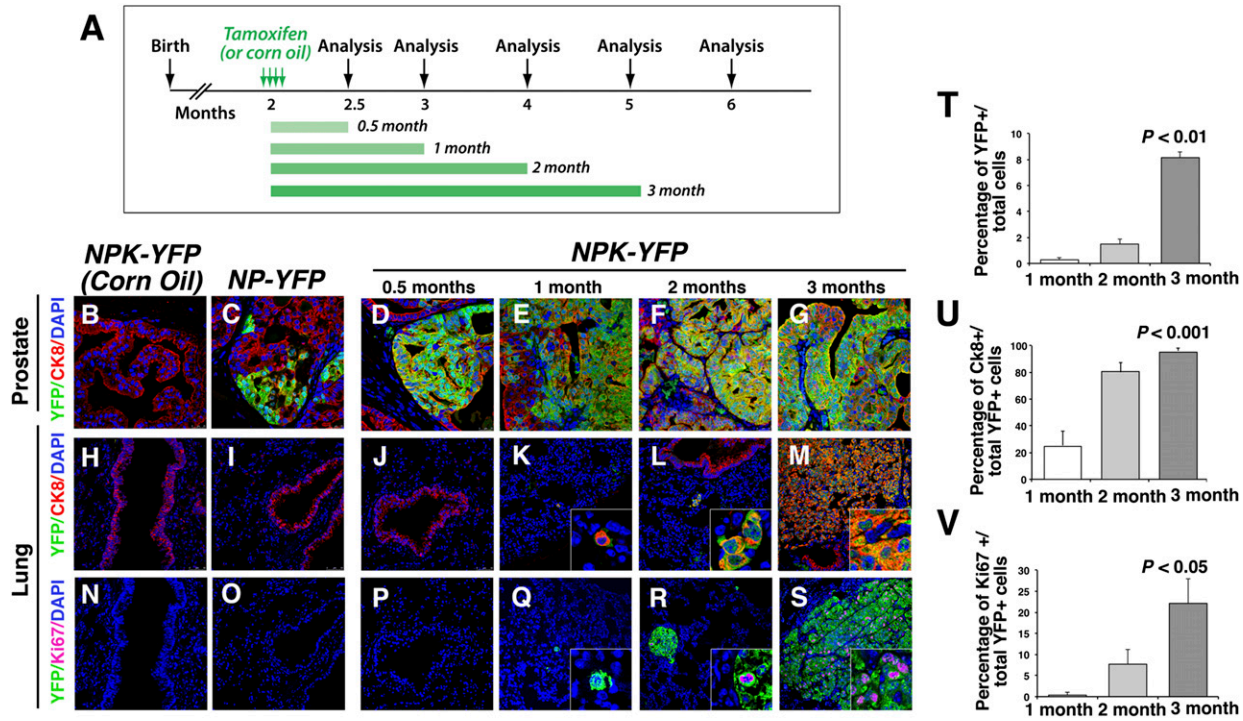

Fig. 6. Lineage-tracing analysis of the spatial and temporal occurrence of metastases. (*A*) Experimental strategy. *NPK-YFP* (or *NP-YFP*) mice were induced with tamoxifen (or treated with corn oil as control) for four consecutive days and then analyzed from 2 wk (0.5 mo) to up to 4 mo following induction. (*B–S*) Representative confocal images of prostate or lungs from *NKP-YFP* mice (or the control *NPK-YFP* treated with corn oil, or *NP-YFP* mice), which were analyzed at the indicated time points following tamoxifen induction. Images show immunofluorescence staining for YFP-expressing cells (green), costained with CK8 (red) or Ki67 (magenta); all cells were visualized with DAPI (blue). (*Insets*) High-power images. (*T–V*) Quantification of YFP-expressing cells from lungs of *NPK-YFP* mice at the indicated time points following tamoxifen induction. (*T*) The percentage of YFP-expressing cells relative to the total cells counted (i.e., DAPI-stained cells). (*U*) The percentage of YFP-expressing cells that costained with CK8. (*V*) The percentage of YFP-expressing cells that costained with Ki67. Quantification of cell-counting data are provided in *SI (Fig. Appendix*, Table S2; additional supporting data are provided in *SI Appendix*, Figs. S3 and S4.

Appendix, Fig. S5*A*). Furthermore, among the oncogenic *Ets* genes, we found that only *Etv4* was significantly up-regulated in both the *NPK* vs. *NP* tumors ($P < 0.001$), as well as in the 3-mo vs. 1-mo *NPK* tumors ($P = 0.0093$; Fig. 7*C*; *SI Appendix*, Fig. S5*B*). In addition, increased expression of Etv4 protein was evident by immunostaining of the primary tumors, as well as lung metastases from the 3-mo *NPK* mice and micrometastases from the 2-mo *NPK* mice (Fig. 7*D*).

To assess the relevance of these findings for human prostate cancer, we examined the relationship of *ETS* gene expression and target gene activation relative to PI3-kinase and Ras signaling in the Taylor human prostate cancer dataset (6). These analyses revealed a significant correlation of *ETV4* expression ($P = 0.004$) and target gene activation ($P = 0.002$) with activation of both PI3-kinase and Ras signaling in human prostate tumors (Fig. 7*E*). In contrast to *ETV4*, the other oncogenic *ETS* genes *ERG*, *ETV1*, and *ETV5* were not correlated with PI3-kinase and Ras signaling (*SI Appendix*, Fig. S5*C*). These findings demonstrate that *ETV4* is specifically up-regulated in advanced prostate tumors that have coactivation of PI3-kinase and Ras signaling.

***Etv4* Promotes Prostate Cancer Metastasis.** To evaluate the functional relevance of *Etv4* for prostate cancer metastasis, we generated cell lines from metastatic prostate tumors from the *NPK-YFP* mice. We then used these cell lines to evaluate the consequences of perturbing *Etv4* expression in cell culture assays of invasiveness and for tumor growth and metastasis in vivo (Fig. 8*A*). For these analyses, we used a cell line, *CASP-NPK-YFP(1)*, that has properties resembling those of the primary tumor, and retains the ability to metastasize to distant sites when engrafted in immunodeficient mice (Fig. 8*K*). In addition, these *CASP-NPK-YFP(1)* cells can be readily tracked in culture as well as in vivo by their YFP expression. Using these cells, we knocked down *Etv4* expression by infection with two independent lentiviral shRNAs for *Etv4*, or a control lentivirus (Fig. 8 *A* and *B*). In culture, knockdown of Etv4 in the *CASP-NPK-YFP(1)* profoundly reduced their tumorigenicity in colony formation assays (ninefold reduction, $P < 0.0001$; Fig. 8 *C* and *D*), as well as their invasiveness in a matrigel invasion assay (ninefold reduction, $P < 0.001$; Fig. 8 *E* and *F*). In addition to these findings in the mouse prostate cancer cells, we observed similar results following knockdown of ETV4 in PC3 human prostate cancer cells (Fig. 8 *G–J*). In particular, knockdown of ETV4 in the PC3 cells reduced their tumorigenicity in colony formation assays by fivefold ($P < 0.0001$; Fig. 8 *G* and *H*), as well as their invasiveness in a matrigel invasion assay by ninefold ($P = 0.003$; Fig. 8 *I* and *J*).

To analyze the consequences of Etv4 knockdown in vivo, we engrafted *CASP-NPK-YFP(1)* cells expressing the control shRNA or the *Etv4* shRNA s.c. into immunodeficient mice and evaluated subsequent tumor growth and metastasis (Fig. 8 *K–M*). Notably, *CASP-NPK-YFP(1)* cells expressing either the control or *Etv4* shRNA developed tumors with equal efficiency and of equivalent size (average weight = 4.5 and 4.4 g, respectively; $n = 10$ mice, $P = 0.8978$; Fig. 8 *K* and *L*). Strikingly, however, *CASP-NPK-YFP (1)* cells expressing the *Etv4* shRNA were severely impaired in their ability to form metastases relative to the control cells (Fig. 8 *K* and *L*). In particular, whereas mice engrafted with cells expressing the control shRNA displayed numerous metastases to the lungs and liver, mice engrafted with cells expressing the *Etv4* shRNA had relatively few and smaller metastases (lung = 39.5 vs. 4.6 metastases per mouse, $n = 10$ mice, $P = 0.009$; liver = 34.2 vs. 6.4 metastases per mouse, $P = 0.004$; $n = 10$ mice; Fig. 8 *K* and *M*).

PNAS PLUS
SEE COMMENTARY
MEDICAL SCIENCES
Downloaded at Palestinian Territory, occupied on November 26, 2021
www.manaraa.com

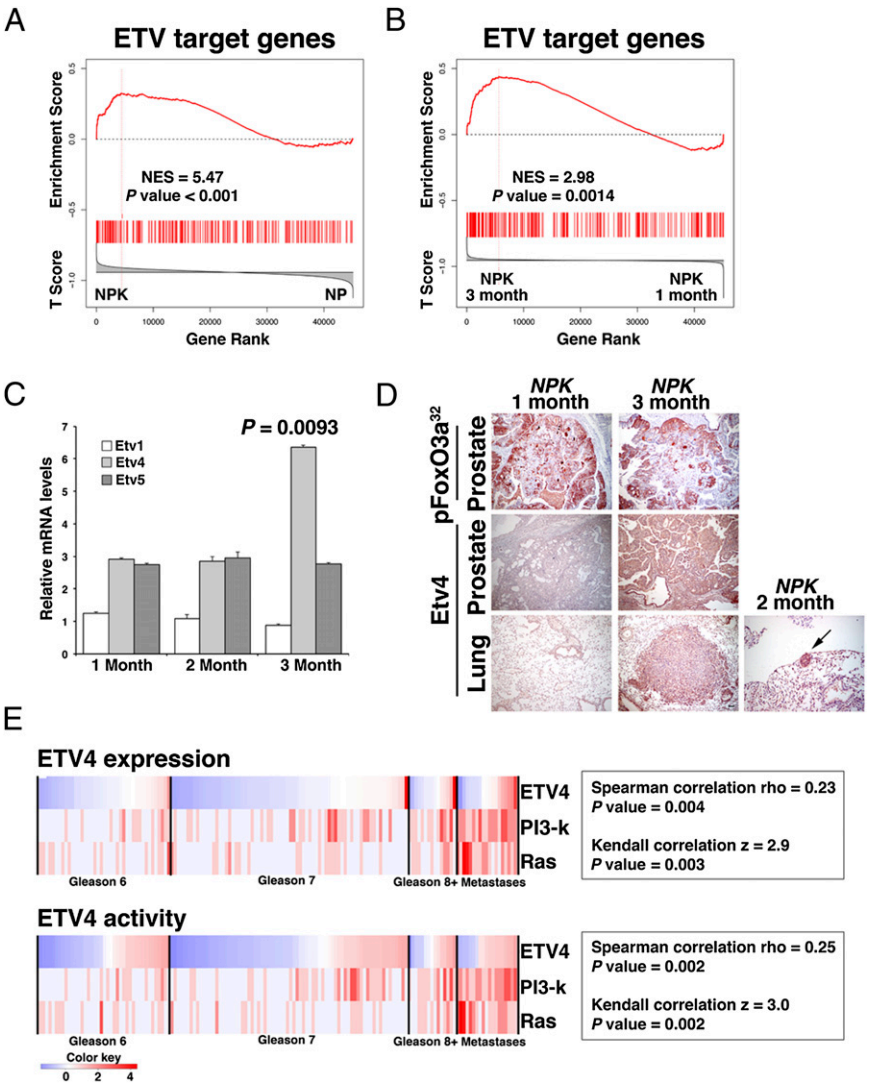

Fig. 7. Activation of *Etv4* by PI3-kinase and Ras signaling in metastatic prostate cancer. (*A* and *B*) GSEA analyses showing enrichment of human *ETV* target genes in reference signatures comparing *NPK* and *NP* mouse prostate tumors (*A*) or 3-mo vs. 1-mo *NPK* mouse prostate tumors (*B*). The mouse genes were mapped to their human orthologs for comparison with a reference signature of human *ETV* target genes. (*C*) Real-time quantitative PCR analyses of *NPK* prostate tumors at 1, 2, or 3 mo following tamoxifen induction showing the relative mRNA expression levels for *Etv1*, *Etv4*, and *Etv5*. *P* value compares the relative levels of *Etv4* at 1 mo vs. 3 mo; other comparisons were not significant. (*D*) Immunostaining of *NPK* prostate tumors or lungs at 1, 2, or 3 mo following tamoxifen induction. Note that the tumor marker pFoxO3a[32] (Fig. 2) is robustly expressed in the prostate tumors at both time points, whereas Etv4 is only expressed in the 3-mo prostate as well as in the lung metastases from this time point as well as the micrometastases at 2 mo. (Scale bars, 100 μm.) (*E*) Correlation of human ETV4 expression and activation of target genes with activation of both PI3-kinase and Ras signaling in human prostate cancer from the Taylor et al. (6) dataset. Shown is a heat map in which the status of ETV4 expression/activity as well as PI3-kinase and Ras signaling activation was evaluated in each of the clinical sample (i.e., primary tumors of the indicated Gleason scores and metastases; *Materials and Methods*). Correlation coefficients, and the *P* values of the correlations, are shown for both Spearman rho and Kendall z calculations. The color key indicates relative expression and activity levels of the ETV4 as well as PI3K and Ras pathways. Additional supporting data are provided in *SI Appendix*, Figs. S5 and S6 and Datasets S4 and S5.

Taken together, these findings demonstrate that *Etv4* promotes prostate cancer metastasis in vivo.

Discussion

Elucidation of the molecular mechanisms of metastasis has been hampered by the lack of appropriate in vivo models for investigation of the relationship among cancer progression, cellular dissemination, and metastases in the context of the native microenvironment. We have performed lineage tracing using a genetically engineered mouse model of metastatic prostate cancer to evaluate the spatial and temporal relationship of tumorigenesis and metastasis in vivo, and to identify molecular pathways that distinguish metastatic tumors. Our findings reveal *ETV4* as a principal driver of metastasis in prostate tumors that have activation of both PI3-kinase and Ras signaling pathways, as frequently occurs in advanced prostate cancer.

One of the principal findings of our study is the observation that cellular dissemination occurs early in prostate tumorigenesis, whereas there is a temporal lag in manifestation of metastases. Notably, in human prostate cancer as many as 70% of patients with localized tumors have disseminated tumor cells in bone marrow before radical prostatectomy, and the presence of such disseminated tumor cells after prostatectomy is associated with increased risk of recurrence (55), which highlights the relevance of our current findings in the *NPK* mouse model for the human disease. Interestingly, an analogous lineage-tracing study of a mouse model of pancreatic cancer, also driven by *Kras*, reported cellular dissemination at early disease stages (56), which was consistent with analyses of human patient samples (57). Furthermore, early dissemination of tumor cells has also been observed in other cancers (58, 59), which suggests the generality of these findings.

Interestingly, our current findings suggest that the disseminated tumor cells that arise before actual metastasis may be dormant, because the solitary tumor cells in the lung are not proliferative. However, at present we cannot determine whether these early disseminating cells are inherently less capable of metastasizing than those that arise later. Our findings demonstrating that metastatic *NPK* prostate tumors have distinct molecular profiles from premetastatic ones suggest that early vs. later disseminated cells may differ in their inherent capacity to metastasize. However, regardless of inherent differences in metastatic potential, it is likely that the ability of disseminated cells to metastasize will be influenced by microenvironment at the metastatic site (1, 3, 4). Notably, though we detect disseminated cells in the bone marrow, we have not observed bone metastases, which may reflect the unfavorable host environment. Indeed, most genetically engineered mouse models of cancer do not develop consistent metastases to bone (45), and the few mouse models of prostate cancer that have reported metastases to bone (60) have

Downloaded at Palestinian Territory, occupied on November 26, 2021
www.manaraa.com

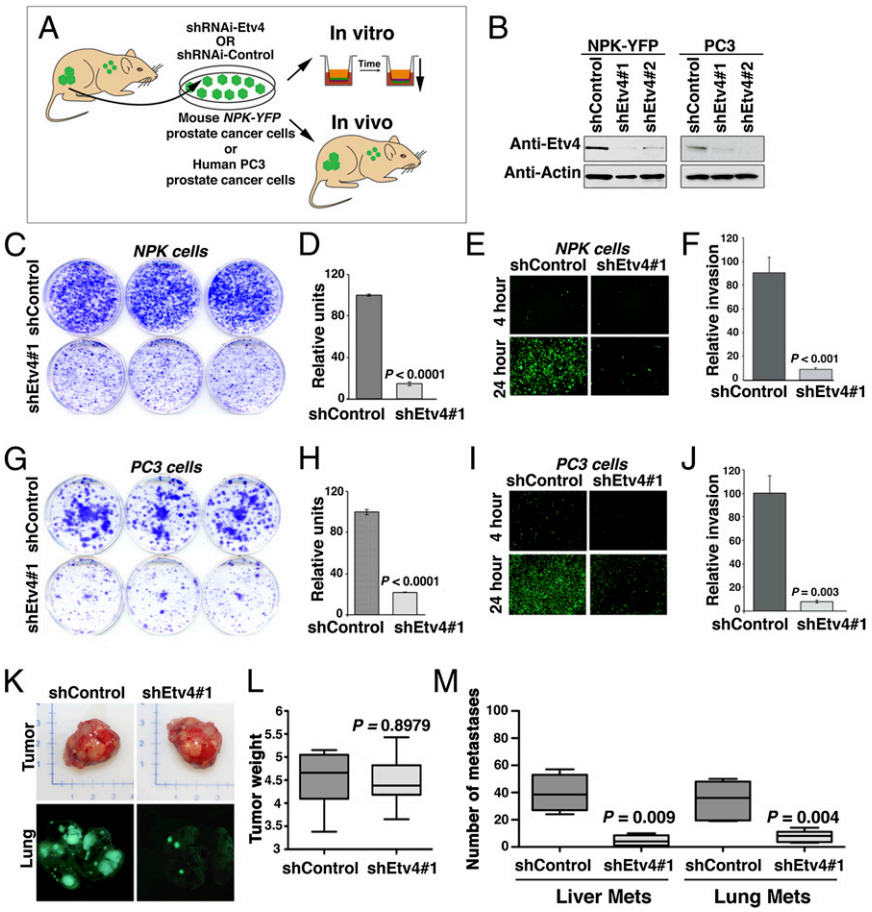

Fig. 8. *Etv4* promotes prostate cancer metastasis. (*A*) Experimental strategy. Cells lines were derived from *NPK-YFP* prostate tumors. The *CASP-NPK-YFP(1)* cells can be visualized by fluorescence by virtue of the expression of YFP, and retain the ability to metastasize when implanted into immunodeficient mice. Cells were infected with lentivirus vector expressing two alternative *Etv4* shRNA or a control shRNA (scrambled sequence). The consequences of *Etv4* knockdown in the experimental vs. control cells were evaluated in vitro, in colony formation, in matrigel invasion assays, as well as in vivo, to quantify the consequences for tumor growth and metastasis. (*B*) Western blot assay showing knockdown of the Etv4 protein with the corresponding shRNA (shEtv4#1 or shEtv4#1) compared with the control (shControl). All assays were done at least three times using both Etv4 shRNA with similar results; the representative data shown were done using shEtv4#1. (*C–J*) In vitro analyses in *CASP-NPK-YFP(1)* (*C–F*) and PC3 (*G–J*) cells. (*C* and *G*) Colony formation assay in cells expressing shControl or shEtv4#1 lentivirus showing representative plates stained with crystal violet. (*D* and *H*) Quantification of colony formation assay data. (*E* and *I*) Matrigel invasion assay in cells expressing shControl or shEtv4#1 lentivirus showing the increased invasion of fluorescent cells expressing the control shRNA but not the *Etv4* shRNA. (*F* and *J*) Quantification of invasion assay data. (*K–M*) In vivo analyses in *CASP-NPK-YFP(1)* cell. (*K*) Images of tumors (*Upper*) and visualization of lung metastases by fluorescence (*Lower*) from immunodeficient mice implanted with *CASP-NPK-YFP(1)* cells expressing the shControl or shEtv4#1 lentivirus. (*L*) Summary of tumor weights (n = 10 mice per group). (*M*) Summary of the total number of metastases per mouse analyzed (n = 10 mice per group) for liver and lung as indicated. In each case, the P values compare the results in cells expressing the shEtv4#1 lentivirus with those expressing the shControl.

been suggested to be due to local invasion rather than actual metastases (61).

Our current findings have established the necessity of *ETV4* for prostate cancer metastases in vivo. *ETV* genes (i.e., members of the *PEA3* subfamily of *ETS* genes) have previously been implicated as transcriptional regulators of cancer invasion and metastasis in various cancer types, and several of their targets include genes associated with metastatic dissemination (51, 52, 62, 63). Furthermore, it has previously been proposed that *ETV4* may be particularly relevant for prostate cancer progression, because it is robustly up-regulated in PC3 human prostate cancer cells, and its depletion in these cells impairs their anchorage-independent growth in cell culture (50). Interestingly, our analysis of *ETV4* target gene activation in human prostate cancer has revealed that *ETV4* is preferentially correlated with PI3-kinase and Ras signaling in bone metastases compared with lymph node metastases (*SI Appendix*, Fig. S6).

Moreover, our findings highlighting a role for *ETV4* in advanced prostate cancer distinguish it from other oncogenic *ETS* genes—namely, *ERG* and *ETV1*, which are activated early in prostate cancer progression and primarily via gene recombination (13–15). Thus, we propose that there may be a cascade of *ETS* gene function in prostate cancer progression, in which the later-acting genes, such as *ETV4*, may be activated not by gene recombination but in response to signaling events. Interestingly, both *ERG* and *ETV1* have been shown to influence the transcriptional program of the androgen receptor (19, 23), which raises the important question of how *ETV4* may interplay with androgen receptor signaling in advanced prostate cancer.

Finally, our current findings shed light on the relationship between oncogenic *ETS* genes and Ras signaling. In particular, our findings highlight a key functional role for *ETV4* in metastatic prostate cancer in response to Ras and PI3-kinase signaling. Given the principal role of Ras signaling in metastases, combined with the fact that Ras signaling is generally refractory to conventional therapy (64, 65), targeting *ETV4* in prostate cancer may provide an alternative means of inhibiting metastasis. This idea is supported by the potential to target the ubiquitin ligase COP1, which has been shown to regulate *ETV* function in prostate cancer (66). Thus, our findings support the idea of targeting *ETV4* as a means of abrogating Ras signaling in advanced prostate cancer.

Materials and Methods

Generation and Analysis of Genetically Engineered Mice. All experiments using animals were performed according to protocols approved by the Institutional Animal Care and Use Committee (IACUC) at Columbia University Medical Center. Mouse alleles were as follows: the *Nkx3.1*$^{CreERT2/+}$ allele, which is null for *Nkx3.1*, expresses Cre-ERT2 under the control of the *Nkx3.1* promoter as reported in ref. 36; a conditional allele for *Pten* (*Pten*$^{flox/flox}$) having loxP sites flanking exon 5 (37) and a lox-stop-lox *Kras*^{G12D} allele expressing an inducible *Kras* allele (38) obtained from the National Cancer Institute Mouse Models of Human Cancer Consortium; and the *R26R-YFP* allele having YFP expressed under the control of the R26R promoter (48), provided by Frank Costantini (Columbia University Medical Center, New York). Mice were maintained on a mixed strain C57BL/6, 129/Sv, and FVB background. For induction of Cre activity, mice were administered tamoxifen (Sigma catalog no. T5648) dissolved in corn oil by oral gavage (100 mg/kg) once daily for four consecutive days, at 2 mo of age. Following tumor induction, mice were monitored daily for body condition (i.e., muscle tone and weight) and killed when their body condition score was <1.5, as per guidelines of the IACUC.

PNAS PLUS
SEE COMMENTARY
MEDICAL SCIENCES
Downloaded at Palestinian Territory, occupied on November 26, 2021
www.manaraa.com

MRI imaging of prostate tumors was done on a 200-MHz Bruker 4.7T BioSpec scanner.

At the time of euthanization, full necropsy was done on each experimental mouse; prostate tissues were collected, photographed, and weights determined. Individual prostatic lobes (anterior, dorsolateral, and ventral) were fixed in 10% (vol/vol) formalin and paraffin-embedded, cryopreserved in optimal cutting-temperature compound, or snap-frozen in liquid nitrogen. In addition to prostate, a spectrum of tissues were collected into 10% formalin for analyses of metastasis, including kidneys, liver, lungs, pancreas, small intestine, heart, lumbar lymph node, caudal lymph node, and submandibular lymph nodes.

Disseminated tumor cells from bone marrow were collected from the femur. Flushed cells were pelleted by centrifugation and digested in lysis buffer [0.5 M KCl, 0.1 M Tris·HCl (pH 8.3), 0.1 mg/mL gelatin, 0.45% Nonidet, 0.45% Tween-20, 0.25 mg/mL of proteinase K]. Extracted DNA was amplified using primers that flank the loxP sites in exon 5 of the *Pten*$^{f/f}$ allele using Platinum Genotype Tsp DNA polymerase (Invitrogen). The presence of the floxed *Pten* allele in genomic DNA from the DTCs was quantified by real-time PCR and normalized to *Gapdh*; relative fold enrichment was calculated using the comparative CT method (ΔΔCT method) and is reported in *SI Appendix*, Table S2. Sequences of the primers used in these studies are provided in *SI Appendix*, Table S3.

Pathological grading was done on H&E-stained slides. Images were captured using an Olympus VS120 whole-slide scanning microscope. Histopathology follows the grading of Park et al. (67). Immunohistochemical and immunofluorescence staining were done on 3-μm paraffin sections as described (36, 68). Primary antibodies and dilutions used are listed in *SI Appendix*, Table S4. For quantification of proliferating cells, slides were immunostained with Ki67, and a minimum of five independent sections from five independent mice (i.e., 25 sections) were counted as done previously (69). Statistical analyses were performed using a two-tailed *t* test, X^2 test, or Fisher's exact test as appropriate. GraphPad Prism software (version 5.0) was used for all statistical analysis and to generate data plots.

Western blot analyses were done using total protein lysates (10 μg per lane) from dorsolateral prostate or prostate tumors. Details of antibodies are provided in *SI Appendix*, Table S4. For analyses of mRNA expression levels using real-time PCR, total RNA was isolated from anterior prostate or prostate tumors using TRIzol reagent (Invitrogen) and real-time quantitative PCR was done using the QuantiTect SYBR Green PCR kit (Qiagen) with *Gapdh* for normalization. Expression ratios of transcripts were tested for significance of differential expression by a pairwise fixed reallocation randomization test using the Relative Expression Software Tool (Qiagen). Sequences of primers are provided in *SI Appendix*, Table S3.

Gene Expression Profiling and Computational Analyses. Total RNA was isolated from mouse prostate tissues using the MagMAX-96 total RNA isolation kit (Ambion), in vitro transcribed to cRNA, and hybridized on mouseWG-6 v2 BeadArrays (Illumina). Data were normalized using standard variance stabilizing transformation (VST) and robust spline normalization functions of R-system v2.11.1 lumi library. Differential gene expression was defined using the Welch *t* test (t.test function in R v2.11.1). Raw and normalized data are available from the Gene Expression Omnibus database (accession no. GSE47697). For cross-species comparison, mouse genes were mapped to human orthologs using mouse–human orthologous relations from the Mouse Genome Informatics database (www.informatics.jax.org).

GSEA (42) was done using sample shuffling where there were more than six samples per group, and gene shuffling if there were fewer than six samples per group for *P* value estimated with 1,000 permutations. Fold-change (FC) analysis for mouse profiles was performed on data regenerated by inverseVST transformation; FC analysis for human was performed on data regenerated by inverse log transformation. Comparison of mouse and human malignancy signatures was done by GSEA using a reference human signature of malignant (Gleason score 8 and 9 with rapid biochemical recurrence within 3 y; n = 10 samples) vs. indolent (i.e., prostate tumors with Gleason score 6 without biochemical recurrence; n = 39 samples) prostate tumors (6).

Phenotypic analyses of biological pathways were done using pathways collected in the REACTOME (70), KEGG (71), and BioCarta (www.biocarta.com/genes/allpathways.asp) databases. To avoid diluting signatures for pathways, including both activated and repressed genes (e.g., positive and negative regulators of cell cycle), ranking by differential expression was performed both using the signed value (i.e., from the most overexpressed to the most underexpressed gene) as well as using the absolute value (i.e., from the most- to the least-differentially expressed gene).

To define alterations in the PI3-kinase and Ras pathways in human samples, we adopted methodology defined in Taylor et al. (6). Gene expression profiles of human primary tumors as well as metastatic samples were normalized by the average of the expression profiles in the adjacent normal samples (normalization was done for each gene), and each sample was scored by the number of gene alterations for PI3-kinase and Ras pathways. As defined in Taylor et al. (6), the PI3-kinase pathway was considered altered if a gene from the pathway (i.e., *PTEN, INPP4B, PIK3R1, PIK3R3, PHLPP, PIK3CA*) was altered, and the Ras signaling pathway was considered altered if a gene from the pathway (i.e., *KRAS, PTPN11, NRAS, BRAF, RAF1, SPRY1, SPRY2*) was altered.

Analyses of *ETS* gene expression were determined for each primary tumor and metastatic sample separately. To estimate an activity profile for the *ETS* gene in each sample, data were normalized to the average of adjacent normal samples (as above), and each tumor sample was then scored with the NES from GSEA mapping-activated (positive) targets of ETS on its normalized gene expression profile. The *ETS* target genes were identified by analyses of a human prostate cancer interactome generated using the ARACNe algorithm (72, 73); the complete interactome will be described elsewhere. To compare discrete (i.e., alteration count) and continuous (i.e., gene expression value) variables, correlations were determined using Spearman's coefficient and then confirmed using Kendall's correlation coefficient.

Functional Analyses in Prostate Cancer Cells. *CASP-NPK-YFP(1)* tumor cells were generated from *NPK-YFP* mice following the method of Speirs et al. (74); a pooled cell population was used for these studies to avoid clonal variation. Once established, the cells were maintained in RMPI with 10% FBS. PC3 cells were obtained from ATCC repository and maintained in RPMI with 10% FBS. For gene knockdown, we used pGIPZ vectors (Open Biosystems) expressing shRNAmirs against mouse (CloneIDs V2LMM_256957 for *Etv4#1* and V3LMM_515851 for *Etv4#2*), human (CloneIDs V3LHS_382918 for *Etv4#1* and V3LHS_382915 for *Etv4#2*), or nontargeting scramble control (RHS4346). Lentiviral particles were made using second-generation packaging vectors and concentrated using the Lenti-X Concentrator reagent (Clontech). Following infection, *CASP-NPK-YFP(1)* or PC3 cells were selected for the presence of the lentivirus using puromycin. In all studies, we used both shEtv#1 and shEtv#2, which gave similar results; shown are representative results using shEtv#1.

Colony formation assays were done using 8×10^3 *CASP-NPK-YFP(1)* or PC3 cells expressing the control or *Etv4* shRNAi lentivirus, which were seeded in triplicate in 60-mm plates and grown for 10 d in RPMI supplemented with 10% FBS. Colonies were visualized by staining with crystal violet and quantified using ImageJ; a Mann–Whitney *U* test was used to calculate the significance (*P* value) of the difference between the control and *Etv4* knockdown cells. Matrigel invasion assays were done using 5×10^4 cells seeded in the BD FluoroBlok inserts (BD Biosciences) in FBS-free media. Inserts were placed in 24-well plates containing RPMI supplemented with 10% FBS as chemoattractant. Invasion was monitored using an inverted fluorescence microscope at 4, 8, 12, 16, 20, and 24 h as detected by YFP expression of the *CASP-NPK-YFP(1)* cells. The fluorescence signal was quantified with ImageJ software, and a Mann–Whitney *U* test was used to calculate the significance (*P* value) of the difference between the control and *Etv4* knockdown cells.

For analyses in vivo, 3×10^6 *CASP-NPK-YFP(1)* cells expressing the control or *Etv4* shRNAi lentivirus were mixed with Matrigel (1:1 vol/vol) and injected into the right flank of immunodeficient NCr *nude* mice (Taconic); tumor growth was monitored for 4 wk. At the time of euthanasia, s.c. tumors were harvested and weighted, and metastases were documented ex vivo in the lungs and livers by visualizing their fluorescence using an Olympus SZX16 microscope equipped with epifluorescence capabilities. The total number of metastatic nodules for the lungs and liver of each mouse was assessed, and the *P* value of the difference between the control and *Etv4* knockdown cells was determined using the Mann–Whitney *U* test.

ACKNOWLEDGMENTS. This work was supported by National Institutes of Health Grants U01 CA084294 (to C.A.-S., M.M.S., and A.C.), P01 CA154293 (to M.M.S. and C.A.-S.), and U54 CA121852 (to A.C.); Silico Research Centre of Excellence National Cancer Institute Cancer Biomedical Informatics Grid (caBIG) Program Science Applications International Corporation (SAIC) 29XS192 (to A.C.); and an award from the V Foundation for Cancer Research (to C.A.-S.). MRI imaging was supported by Grants P50-CA092629 and P30-CA08748 (to J.A.K.). A.A. is the recipient of the Marie Curie International Outgoing Fellowship PIOF-GA-2009-253290, cosponsored with the Catalan Institute of Oncology–Bellvitge Institute for Biomedical Research. C.A.-S. is an American Cancer Society Research Professor supported in part by a generous gift from the F. M. Kirby Foundation.

Downloaded at Palestinian Territory, occupied on November 26, 2021
www.manaraa.com

1. Valastyan S, Weinberg RA (2011) Tumor metastasis: Molecular insights and evolving paradigms. *Cell* 147(2):275–292.
2. Nguyen DX, Bos PD, Massagué J (2009) Metastasis: From dissemination to organ-specific colonization. *Nat Rev Cancer* 9(4):274–284.
3. Joyce JA, Pollard JW (2009) Microenvironmental regulation of metastasis. *Nat Rev Cancer* 9(4):239–252.
4. Kang Y, Pantel K (2013) Tumor cell dissemination: Emerging biological insights from animal models and cancer patients. *Cancer Cell* 23(5):573–581.
5. American Cancer Society (2012) *Cancer Facts and Figures 2012*. Available at www.cancer.org/acs/groups/content/@epidemiologysurveilance/documents/acspc-031941.pdf. Accessed September 25, 2012.
6. Taylor BS, et al. (2010) Integrative genomic profiling of human prostate cancer. *Cancer Cell* 18(1):11–22.
7. Berger MF, et al. (2011) The genomic complexity of primary human prostate cancer. *Nature* 470(7333):214–220.
8. Grasso CS, et al. (2012) The mutational landscape of lethal castration-resistant prostate cancer. *Nature* 487(7406):239–243.
9. Barbieri CE, et al. (2012) Exome sequencing identifies recurrent SPOP, FOXA1 and MED12 mutations in prostate cancer. *Nat Genet* 44(6):685–689.
10. Baca SC, et al. (2013) Punctuated evolution of prostate cancer genomes. *Cell* 153(3):666–677.
11. Abate-Shen C, Shen MM, Gelmann E (2008) Integrating differentiation and cancer: The Nkx3.1 homeobox gene in prostate organogenesis and carcinogenesis. *Differentiation* 76(6):717–727.
12. Shen MM, Abate-Shen C (2010) Molecular genetics of prostate cancer: New prospects for old challenges. *Genes Dev* 24(18):1967–2000.
13. Rubin MA, Maher CA, Chinnaiyan AM (2011) Common gene rearrangements in prostate cancer. *J Clin Oncol* 29(27):3659–3668.
14. Tomlins SA, et al. (2005) Recurrent fusion of TMPRSS2 and ETS transcription factor genes in prostate cancer. *Science* 310(5748):644–648.
15. Clark JP, Cooper CS (2009) ETS gene fusions in prostate cancer. *Nat Rev Urol* 6(8):429–439.
16. Zong Y, et al. (2009) ETS family transcription factors collaborate with alternative signaling pathways to induce carcinoma from adult murine prostate cells. *Proc Natl Acad Sci USA* 106(30):12465–12470.
17. Carver BS, et al. (2009) Aberrant ERG expression cooperates with loss of PTEN to promote cancer progression in the prostate. *Nat Genet* 41(5):619–624.
18. King JC, et al. (2009) Cooperativity of TMPRSS2-ERG with PI3-kinase pathway activation in prostate oncogenesis. *Nat Genet* 41(5):524–526.
19. Chen Y, et al. (2013) ERG reprograms the AR cistrome and primes prostate tumorigenesis in response to PTEN loss. *Nat Med* 19(8):1023–1029.
20. Oh S, Shin S, Janknecht R (2012) ETV1, 4 and 5: An oncogenic subfamily of ETS transcription factors. *Biochim Biophys Acta* 1826(1):1–12.
21. Tomlins SA, et al. (2007) Distinct classes of chromosomal rearrangements create oncogenic ETS gene fusions in prostate cancer. *Nature* 448(7153):595–599.
22. Tomlins SA, et al. (2006) TMPRSS2:ETV4 gene fusions define a third molecular subtype of prostate cancer. *Cancer Res* 66(7):3396–3400.
23. Baena E, et al. (2013) ETV1 directs androgen metabolism and confers aggressive prostate cancer in targeted mice and patients. *Genes Dev* 27(6):683–698.
24. Scher HI, Sawyers CL (2005) Biology of progressive, castration-resistant prostate cancer: Directed therapies targeting the androgen-receptor signaling axis. *J Clin Oncol* 23(32):8253–8261.
25. Shen MM, Abate-Shen C (2007) Pten inactivation and the emergence of androgen-independent prostate cancer. *Cancer Res* 67(14):6535–6538.
26. Voeller HJ, Wilding G, Gelmann EP (1991) v-rasH expression confers hormone-independent in vitro growth to LNCaP prostate carcinoma cells. *Mol Endocrinol* 5(2):209–216.
27. Bakin RE, Gioeli D, Bissonette EA, Weber MJ (2003) Attenuation of Ras signaling restores androgen sensitivity to hormone-refractory C4-2 prostate cancer cells. *Cancer Res* 63(8):1975–1980.
28. Carracedo A, Pandolfi PP (2008) The PTEN-PI3K pathway: Of feedbacks and cross-talks. *Oncogene* 27(41):5527–5541.
29. Weber MJ, Gioeli D (2004) Ras signaling in prostate cancer progression. *J Cell Biochem* 91(1):13–25.
30. Prior IA, Lewis PD, Mattos C (2012) A comprehensive survey of Ras mutations in cancer. *Cancer Res* 72(10):2457–2467.
31. Carter BS, Epstein JI, Isaacs WB (1990) Ras gene mutations in human prostate cancer. *Cancer Res* 50(21):6830–6832.
32. Moul JW, Friedrichs PA, Lance RS, Theune SM, Chang EH (1992) Infrequent RAS oncogene mutations in human prostate cancer. *Prostate* 20(4):327–338.
33. Gumerlock PH, Poonamallee UR, Meyers FJ, deVere White RW (1991) Activated ras alleles in human carcinoma of the prostate are rare. *Cancer Res* 51(6):1632–1637.
34. Wang XS, et al. (2011) Characterization of KRAS rearrangements in metastatic prostate cancer. *Cancer Discov* 1(1):35–43.
35. Sboner A, et al. (2010) Molecular sampling of prostate cancer: A dilemma for predicting disease progression. *BMC Med Genomics* 3:8.
36. Wang X, et al. (2009) A luminal epithelial stem cell that is a cell of origin for prostate cancer. *Nature* 461(7263):495–500.
37. Lesche R, et al. (2002) Cre/loxP-mediated inactivation of the murine Pten tumor suppressor gene. *Genesis* 32(2):148–149.
38. Jackson EL, et al. (2001) Analysis of lung tumor initiation and progression using conditional expression of oncogenic K-ras. *Genes Dev* 15(24):3243–3248.
39. Mulholland DJ, et al. (2012) Pten loss and RAS/MAPK activation cooperate to promote EMT and metastasis initiated from prostate cancer stem/progenitor cells. *Cancer Res* 72(7):1878–1889.
40. Ouyang X, et al. (2008) Activator protein-1 transcription factors are associated with progression and recurrence of prostate cancer. *Cancer Res* 68(7):2132–2144.
41. Min J, et al. (2010) An oncogene-tumor suppressor cascade drives metastatic prostate cancer by coordinately activating Ras and nuclear factor-kappaB. *Nat Med* 16(3):286–294.
42. Subramanian A, et al. (2005) Gene set enrichment analysis: A knowledge-based approach for interpreting genome-wide expression profiles. *Proc Natl Acad Sci USA* 102(43):15545–15550.
43. Gupta S, et al. (2007) Binding of ras to phosphoinositide 3-kinase p110alpha is required for ras-driven tumorigenesis in mice. *Cell* 129(5):957–968.
44. Dansen TB, Burgering BM (2008) Unravelling the tumor-suppressive functions of FOXO proteins. *Trends Cell Biol* 18(9):421–429.
45. Irshad S, Abate-Shen C (2013) Modeling prostate cancer in mice: Something old, something new, something premalignant, something metastatic. *Cancer Metastasis Rev* 32(1-2):109–122.
46. Wang J, et al. (2012) B-Raf activation cooperates with PTEN loss to drive c-Myc expression in advanced prostate cancer. *Cancer Res* 72(18):4765–4776.
47. Logothetis CJ, Lin SH (2005) Osteoblasts in prostate cancer metastasis to bone. *Nat Rev Cancer* 5(1):21–28.
48. Srinivas S, et al. (2001) Cre reporter strains produced by targeted insertion of EYFP and ECFP into the ROSA26 locus. *BMC Dev Biol* 1:4.
49. Hollenhorst PC, et al. (2011) Oncogenic ETS proteins mimic activated RAS/MAPK signaling in prostate cells. *Genes Dev* 25(20):2147–2157.
50. Hollenhorst PC, Paul L, Ferris MW, Graves BJ (2011) The ETS gene *ETV4* is required for anchorage-independent growth and a cell proliferation gene expression program in PC3 prostate cells. *Genes Cancer* 1(10):1044–1052.
51. Keld R, et al. (2011) PEA3/ETV4-related transcription factors coupled with active ERK signalling are associated with poor prognosis in gastric adenocarcinoma. *Br J Cancer* 105(1):124–130.
52. Keld R, et al. (2010) The ERK MAP kinase-PEA3/ETV4-MMP-1 axis is operative in oesophageal adenocarcinoma. *Mol Cancer* 9:313.
53. Rachagani S, et al. (2011) Activated KrasG^{12}D is associated with invasion and metastasis of pancreatic cancer cells through inhibition of E-cadherin. *Br J Cancer* 104(6):1038–1048.
54. Yuen HF, et al. (2011) Polyomavirus enhancer activator 3 protein promotes breast cancer metastatic progression through Snail-induced epithelial-mesenchymal transition. *J Pathol* 224(1):78–89.
55. Morgan TM, et al. (2009) Disseminated tumor cells in prostate cancer patients after radical prostatectomy and without evidence of disease predicts biochemical recurrence. *Clin Cancer Res* 15(2):677–683.
56. Rhim AD, et al. (2012) EMT and dissemination precede pancreatic tumor formation. *Cell* 148(1-2):349–361.
57. Campbell PJ, et al. (2010) The patterns and dynamics of genomic instability in metastatic pancreatic cancer. *Nature* 467(7319):1109–1113.
58. Eyles J, et al. (2010) Tumor cells disseminate early, but immunosurveillance limits metastatic outgrowth, in a mouse model of melanoma. *J Clin Invest* 120(6):2030–2039.
59. Hüsemann Y, et al. (2008) Systemic spread is an early step in breast cancer. *Cancer Cell* 13(1):58–68.
60. Ding Z, et al. (2012) Telomerase reactivation following telomere dysfunction yields murine prostate tumors with bone metastases. *Cell* 148(5):896–907.
61. Ittmann M, et al. (2013) Animal models of human prostate cancer: The consensus report of the New York meeting of the Mouse Models of Human Cancers Consortium Prostate Pathology Committee. *Cancer Res* 73(9):2718–2736.
62. de Launoit Y, et al. (2006) The Ets transcription factors of the PEA3 group: Transcriptional regulators in metastasis. *Biochim Biophys Acta* 1766(1):79–87.
63. Zabuawala T, et al. (2010) An ets2-driven transcriptional program in tumor-associated macrophages promotes tumor metastasis. *Cancer Res* 70(4):1323–1333.
64. Pylayeva-Gupta Y, Grabocka E, Bar-Sagi D (2011) RAS oncogenes: Weaving a tumorigenic web. *Nat Rev Cancer* 11(11):761–774.
65. Downward J (2003) Targeting RAS signalling pathways in cancer therapy. *Nat Rev Cancer* 3(1):11–22.
66. Vitari AC, et al. (2011) COP1 is a tumour suppressor that causes degradation of ETS transcription factors. *Nature* 474(7351):403–406.
67. Park JH, et al. (2002) Prostatic intraepithelial neoplasia in genetically engineered mice. *Am J Pathol* 161(2):727–735.
68. Kinkade CW, et al. (2008) Targeting AKT/mTOR and ERK MAPK signaling inhibits hormone-refractory prostate cancer in a preclinical mouse model. *J Clin Invest* 118(9):3051–3064.
69. Bhatia-Gaur R, et al. (1999) Roles for Nkx3.1 in prostate development and cancer. *Genes Dev* 13(8):966–977.
70. Croft D, et al. (2011) Reactome: A database of reactions, pathways and biological processes. *Nucleic Acids Res* 39(Database issue):D691–D697.
71. Ogata H, et al. (1999) KEGG: Kyoto Encyclopedia of Genes and Genomes. *Nucleic Acids Res* 27(1):29–34.
72. Basso K, et al. (2005) Reverse engineering of regulatory networks in human B cells. *Nat Genet* 37(4):382–390.
73. Margolin AA, et al. (2006) Reverse engineering cellular networks. *Nat Protoc* 1(2):662–671.
74. Speirs V, et al. (1998) Short-term primary culture of epithelial cells derived from human breast tumours. *Br J Cancer* 78(11):1421–1429.

PNAS PLUS
SEE COMMENTARY
MEDICAL SCIENCES
Downloaded at Palestinian Territory, occupied on November 26, 2021
www.manaraa.com